Two Distinct Ca^{2+}-Dependent Signaling Pathways Regulate the Motor Output of Cochlear Outer Hair Cells

Gregory I. Frolenkov,[1] Fabio Mammano,[2] Inna A. Belyantseva,[1] Donald Coling,[1] and Bechara Kachar[1]

[1]*Section on Structural Cell Biology, National Institute on Deafness and Other Communication Disorders, National Institutes of Health, Bethesda, Maryland 20892-4163, and* [2]*Laboratory of Biophysics and Istituto Nazionale di Fisica della Materia, International School for Advanced Studies, via Beirut 2-4, 34014, Trieste, Italy*

The outer hair cells (OHCs) of the cochlea have an electromotility mechanism, based on conformational changes of voltage-sensitive "motor" proteins in the lateral plasma membrane. The translocation of electrical charges across the membrane that accompanies electromotility imparts a voltage dependency to the membrane capacitance. We used capacitance measurements to investigate whether electromotility may be influenced by different manipulations known to affect intracellular Ca^{2+} or Ca^{2+}-dependent protein phosphorylation. Application of acetylcholine (ACh) to the synaptic pole of isolated OHCs evoked a Ca^{2+}-activated apamin-sensitive outward K^+ current. It also enhanced electromotility, probably because of a phosphorylation-dependent decrease of the cell's axial stiffness. However, ACh did not change the voltage-dependent capacitance either in conventional whole-cell experiments or under perforated-patch conditions. The effects produced by the Ca^{2+} ionophore ionomycin mimicked those produced by ACh. Hyperpolarizing shifts of the voltage dependence of capacitance and electromotility were induced by okadaic acid, a promoter of protein phosphorylation, whereas trifluoperazine and W-7, antagonists of calmodulin, caused opposite depolarizing shifts. Components of the protein phosphorylation cascade—IP_3 receptors and calmodulin-dependent protein kinase type IV—were immunolocalized to the lateral wall of the OHC. Our results suggest that two different Ca^{2+}-dependent pathways may control the OHC motor output. The first pathway modulates cytoskeletal stiffness and can be activated by ACh. The second pathway shifts the voltage sensitivity of the OHC electromotile mechanism and may be activated by the release of Ca^{2+} from intracellular stores located in the proximity of the lateral plasma membrane.

Key words: sensory transduction; electromotility; voltage-dependent capacitance; cochlea; endoplasmic reticulum; patch clamp; organ of Corti

Outer hair cells (OHCs)—the sensorimotor receptors of the mammalian cochlea—elongate and shorten at acoustic frequencies when their intracellular potential is changed (for review, see Dallos, 1992; Frolenkov et al., 1998a). This unique property turns OHCs into active devices that amplify the sound-evoked mechanical responses of the organ of Corti. The ability of OHCs to change shape in a voltage-dependent manner is generally referred to as *electromotility* and is presumably based on voltage-driven conformational changes of densely packed putative "motor" proteins in the lateral plasma membrane (Kalinec et al., 1992). These conformational changes entail the translocation of electrical charges across the plasma membrane, observed as fast transient currents at the onset and offset of transmembrane voltage steps (Santos-Sacchi, 1991) similar to the "gating" currents recorded from voltage-dependent ion channels. However, the conformational changes of the OHC motor proteins are not associated with a net ion flow across the membrane (Santos-Sacchi and Dilger, 1988) but produce changes in the surface area of the membrane (Kalinec et al., 1992). The motor's charge movement is sensitive to chemicals inhibiting OHC electromotility (Tunstall et al., 1995; Kakehata and Santos-Sacchi, 1996). It commonly saturates for membrane voltages below −120 mV and above +80 mV, which imparts a bell-shaped dependence to the membrane capacitance (Santos-Sacchi, 1991).

Clearly, electromotility involves a novel mechanism of force production distinct from conventional ATP-dependent, cytoskeletal-based contractile processes (Kachar et al., 1986). Nonetheless, the cylindrical shape of OHCs is maintained by a cortical cytoskeleton (Holley et al., 1992), and the elongation produced in OHCs by the Ca^{2+} ionophore ionomycin has been attributed to a Ca^{2+}/calmodulin-dependent phosphorylation of cytoskeletal proteins (Dulon et al., 1990; Coling et al., 1998).

OHCs are the target of an efferent innervation originating in the brainstem (Warr, 1992). The principal neurotransmitter of this efferent system is acetylcholine (ACh) (Eybalin, 1993). Whole-cell recordings from isolated OHCs have provided evidence of cholinergic receptors localized around the base of the cell, where the efferent synapses are located (Housley and Ashmore, 1991). The action of ACh on OHCs requires extracellular Ca^{2+} (Blanchet et al., 1996; Evans, 1996), is accompanied by changes of intracellular free Ca^{2+} concentration ($[Ca^{2+}]_i$) (Doi and Ohmori, 1993), and is mediated by a novel receptor, named the $\alpha 9$ ACh receptor (Elgoyhen et al., 1994). Recently Dallos et al. (1997) showed that ACh increases the electromotile responses of OHCs and attributed this effect to a decreased axial stiffness, presumably mediated by Ca^{2+}-dependent phosphorylation of unspecified cytoskeletal proteins (Szonyi et al., 1999). The molecular targets of these Ca^{2+}-mediated intracellular cascades remain difficult to identify because the OHC axial stiffness depends also on the transmembrane potential (Frolenkov et al., 1998b; He and Dallos, 1999). This suggests that the motor output of OHC can be modulated by regulatory mechanisms that target both the cytoskeleton and the membrane motor proteins.

In the present study we used capacitance measurements to investigate whether the voltage-sensitive membrane component of the OHC electromotility mechanism can be directly affected by intracellular Ca^{2+} or by Ca^{2+}-dependent signaling pathways involving protein phosphorylation.

MATERIALS AND METHODS

Cell preparation. Adult guinea pigs (200–400 gm) were killed by suffocation with carbon dioxide and decapitated. The temporal bones were removed

Received Dec. 6, 1999; revised May 24, 2000; accepted May 25, 2000.

This work was supported in part by a grant to F.M. from Istituto Nazionale di Fisica della Materia (Progetto di Ricerca Avanzata CADY). We thank Robert Fettiplace and Kuni Iwasa for critical comments and helpful suggestions.

Correspondence should be addressed to Dr. Bechara Kachar, Section on Structural Cell Biology, National Institute on Deafness and Other Communication Disorders, National Institutes of Health, Building 36, Room 5D15, Bethesda, MD 20892-4163. E-mail: kacharb@nidcd.nih.gov.

 0270-6474/00/205940-09$15.00/0

from the skull and placed in modified Leibovitz cell culture medium (L-15) containing the following inorganic salts (in mM): NaCl (138), KCl (5.3), $CaCl_2$ (1.26), $MgCl_2$ (1.0), Na_2HPO_4 (1.34), KH_2PO_4 (0.44), and $MgSO_4$ (0.81). For some experiments, a solution designed to block most of the membrane conductance was used, containing (in mM): NaCl (142), KCl (5.4), $CaCl_2$ (1.3), $MgCl_2$ (1.5), HEPES (5), tetraethylammonium chloride (20), CsCl (20), and $CoCl_2$ (2). The osmolarity of the extracellular solutions was adjusted to 325 ± 2 mOsm with D-glucose or D-galactose, and the pH was adjusted to 7.4 with NaOH. To isolate OHCs, we opened the bulla to expose the cochlea and chipped away the otic capsula with a surgical blade, starting from the base. Strips of the organ of Corti were dissected from the modiolus with a fine needle, transferred with a glass pipette to a 100 μl drop of medium containing 1 mg/ml collagenase type IV (Life Technologies, Rockville, MD), and kept there for 15–20 min. In some experiments, the strips were preincubated (30–60 min at 37°C) with drugs affecting protein phosphorylation: okadaic acid, trifluoperazine, and W-7 (Calbiochem, San Diego, CA). As controls for these experiments, cells were maintained in the L-15 medium for the same amount of time. After incubation, cells were dissociated by gentle reflux of the tissue through the needle of a Hamilton syringe (705; 22 gauge) and allowed to settle on the slide for 5–10 min. During the experiment, cells were placed in a laminar flow bath (100 μl), with exchange of solution (~5 ml/hr) by a pressurized perfusion system (BPS-4; ALA Scientific Instruments, Westbury, NY). OHCs were maintained at room temperature (22–24°C) throughout the experiments.

Patch-clamp recordings. As a result of the enzymatic treatment and mechanical dissociation, isolated OHCs showed different degrees of cell damage. This required careful selection of the cells before patch clamping. No reports exist in the literature that allowed the comparison of differential interference contrast images of OHCs *in situ* with isolated ones. Therefore we relied on the several years of experience of these laboratories to determine cell viability based on the following morphological features: uniform cylindrical shape, basal location of the nucleus, membrane birefringence, and intact stereocilia. Shorter cells (34–52 μm) were used for experiments involving the pressure application of acetylcholine, and longer cells (40–79 μm) were used for the other experiments. Pipettes for conventional or perforated-patch (Horn and Marty, 1988) whole-cell recordings were formed on a programmable puller (P87; Sutter Instruments, Novato, CA) from 1.0 mm outer diameter borosilicate glass (#30-30-0; FHC, Bowdoinham, ME). For conventional patch-clamp recordings, pipettes were filled with an intracellular solution containing (in mM): KCl (144), $MgCl_2$ (2.0), EGTA (0.5), Na_2HPO_4 (8.0), NaH_2PO_4 (2.0), Mg-ATP (2.0), and Na-GTP (0.2), adjusted to pH 7.4 with KOH and brought to 325 mOsm with D-glucose. When using ion channel blockers in the extracellular medium, pipettes were filled with (in mM): CsCl (140), $MgCl_2$ (2.0), EGTA (5.0), HEPES (5), Mg-ATP (2.0), and Na-GTP (0.2), adjusted to pH 7.4 with CsOH and brought to 325 mOsm with D-glucose.

For perforated-patch recordings the pipette solution contained 150 mM KCl, 10 mM HEPES (buffered with Tris-hydroxymethyl-aminomethane to pH 7.2), 500 μg/ml nystatin (Calbiochem), and 200 μg/ml fluoresceine (Molecular Probes, Eugene, OR). Both nystatin and fluoresceine were freshly predissolved in DMSO to make 50 and 20 mg/ml stock solutions, respectively. Before filling the pipette with the nystatin-containing solution, its tip was loaded with a small volume of nystatin- and DMSO-free solution to avoid interference with seal formation. After seal formation, the progress of perforation was assayed by monitoring the capacitive current transients evoked by 5 mV steps. At the end of perforated-patch experiments, we recorded the image of the OHC under epifluorescent illumination before and after breaking the perforated patch with negative pressure. Fluorescent signals were detected from the cell only after breaking the patch, indicating that the perforated patch had excluded the passage of substances with a molecular weight comparable with, or larger than, that of the fluorescent probes.

Patch-clamp recordings were performed using an Axopatch 1D amplifier (Axon Instruments, Foster City, CA). Current and voltage were sampled at 100 kHz using a standard laboratory interface (Digidata 1200A; Axon Instruments) controlled by pCLAMP 7.0 software (Axon Instruments). The uncompensated pipette resistance was typically 3–5 MΩ when measured in the bath. The access resistance did not exceed 15 MΩ under conventional and 25 MΩ under perforated-patch conditions. Potentials were corrected off-line for the error caused by the access resistance. Junction potentials were −4.2 mV for the conventional intracellular and extracellular solution combination and −5.3 mV for the ion channel-blocking combination, as computed by the pCLAMP 7.0 software on the basis of the given solution composition. These values were very similar and rather small; therefore no correction was applied to the data for liquid junction potentials.

Drug delivery. A puff pipette, prepared similarly to the patch pipette, was filled with ACh (Sigma, St. Louis, MO) or ionomycin (Calbiochem) dissolved in the extracellular solution. It was placed near the synaptic pole (ACh; Fig. 1*A*) or the lateral wall (ionomycin) of the OHC, and 10 kPa of pressure was applied to its back by a pneumatic injection system (PLI-100; Medical Systems Corporation, Greenvale, NY) gated under software control.

Capacitance measurement. Measurements of cell capacitance were performed using the "membrane test" feature of the pCLAMP 7.0 acquisition software, which continuously delivered a test square wave of period $T = 4$ msec to the cell, through the patch-clamp amplifier. This produced transient currents that decayed exponentially with time constant τ (Fig. 1*B*, *top left*). The software was designed for the simultaneous on-line measurement of τ, the total resistance R_t seen by the amplifier, and the electrical charge delivered to the membrane capacitance C_m. Unfortunately the pCLAMP software accurately estimates the parameters cell membrane resistance (R_m), pipette access resistance (R_a), and C_m only if $R_m \gg R_a$, a condition that was not always met. To circumvent this problem, we reversed off-line the pCLAMP algorithm to recover the original values for the time integral of the transient current Q and R_t. We then recomputed R_m, R_a, and C_m according to the equations shown below. The simplified electrical circuit used to represent a patch-clamped OHC is shown in Figure 1*B*, *top right*. The voltage step V elicited a whole-cell current:

$$i = \frac{V}{R_m + R_a}\left[1 + \frac{R_m}{R_a}\exp(-t/\tau)\right],$$

where:

$$\tau = \frac{R_m R_a}{R_m + R_a} C_m . \quad (1)$$

The charge delivered to the equivalent circuit by the transient current is:

$$Q = \int_0^{T/2} \frac{V R_m}{(R_m + R_a) R_a}\exp(-t/\tau)\mathrm{d}t =$$

$$= V C_m \left(\frac{R_m}{R_m + R_a}\right)^2 [1 - \exp(-T/2\tau)], \quad (2)$$

and the total resistance is:

$$R_t = R_m + R_a . \quad (3)$$

Solving simultaneously Equations 1–3 yields:

$$R_a = \frac{R_t}{1 + \dfrac{Q R_t}{\tau V[1 - \exp(-T/2\tau)]}}; \quad R_m = R_t - R_a;$$

$$C_m = \frac{Q}{V}\left(\frac{R_t}{R_m}\right)^2 \frac{1}{1 - \exp(-T/2\tau)}.$$

Because the time constant τ of the patch-clamp amplifier was typically in the range 0.1–0.3 msec at holding potentials from −50 to −70 mV, >99.8% of the current had settled within $T/2 = 2$ msec.

The patch-clamp parameters were continuously monitored at a resolution of 25 Hz, by averaging the responses to 10 positive and 10 negative consecutive test steps. The series resistance and linear capacitance compensation circuitry of the patch-clamp amplifier were not used. Instead, to determine the voltage dependence of C_m, we applied triangular voltage ramps, swinging the cell potential from V_h − 100 mV to V_h + 160 mV (where V_h is the holding potential) in 6 sec (Fig. 1*C*). Measured values of R_t were corrected for the slope of the ramp. To test the accuracy of this procedure, we performed measurements of C_m on a model electrical circuit (Fig. 1*B*, *top right*), in which we varied R_m from 500 to 5 MΩ keeping R_a = 10 MΩ constant and C_m equal to one of three values: 10, 20, or 30 pF. The values of C_m, calculated according to the above procedure, differed from their nominal values by no > 4 pF, provided that $R_m/R_t > 0.5$ (Fig. 1*B*, *bottom*). Large errors in the C_m estimate occurred at high R_m/R_t values because the amplitude of the exponentially decaying transient current was less than the steady-state current response to the test step. Under these conditions, the pCLAMP algorithm was unable to "lock" the exponential decay to calculate its time constant.

Generally, we halted data gathering when the ratio R_m/R_t fell < 0.5. In this paper we report only data from cells with voltage-independent (linear) capacitance > 15 pF and $R_m/R_t > 0.6$. Therefore, the maximum error in the estimate of C_m was < 16%. The values of C_m, calculated according to the above procedure, did not change significantly when the voltage was commanded to follow a ramp (Fig. 1*B*, *middle*). Measurements of the cell capacitance during test ramps were corrected for the voltage drop along the access resistance of the pipette and then fitted with:

$$C_m(V) = C_0 + 4C_{\max}\frac{\exp(-(V - V_p)/W)}{[1 + \exp(-(V - V_p)/W)]^2},$$

which is the derivative of a Boltzmann function. C_0 is the linear (voltage-independent) capacitance, C_{max} is the maximum nonlinear capacitance, V_p is the potential at the peak of $C_m(V)$, and $W = k_B T/ze$ is a constant. The latter is a measure of the sensitivity of the nonlinear charge displacement to potential, expressed in terms of a charge of valence z moving from the inner to the outer aspect of the plasma membrane. k_B is Boltzmann's constant, T is absolute temperature, and e is the electron charge.

The voltage-independent fraction of the cell capacitance scales linearly

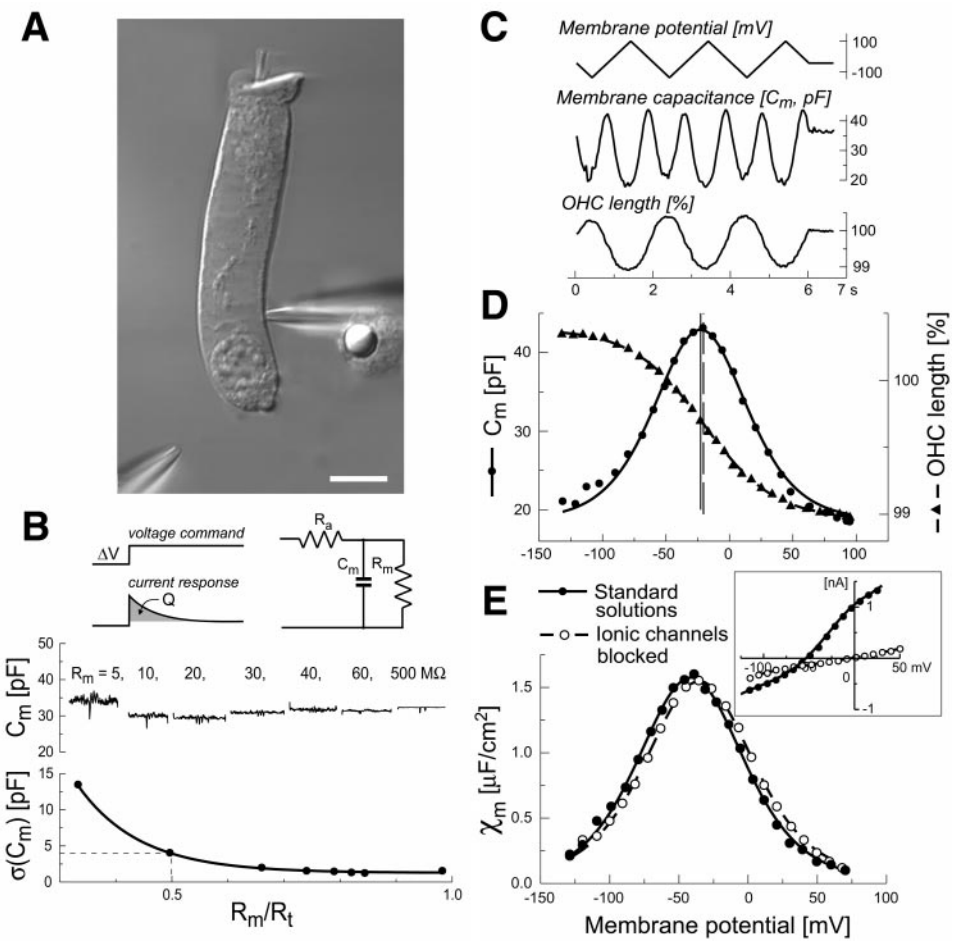

Figure 1. A, Video image to indicate how ACh was delivered to isolated OHCs *in vitro*. The cell was patch-clamped near its nuclear region by a pipette entering from the *right*. A second pipette was positioned close to the cell's synaptic pole for the focal pressure application of ACh. Scale bar, 10 μm. *B, Top left,* Brief voltage steps (square wave; amplitude, 5 mV; frequency, 500 Hz) applied by the patch-clamp amplifier, eliciting transient capacitive currents that were not compensated by the amplifier's circuitry. *Top right,* Scheme of the idealized circuit representing the capacitive cell response. C_m, Membrane capacitance; R_a, pipette access resistance; R_m, cell membrane resistance. *Middle,* Responses of a model electrical circuit used to test the reliability of the capacitance measurements for various values of R_m, displayed above the recordings, while keeping C_m = 30 pF and R_a = 10 MΩ constant. Approximately at the middle of each step, the voltage was ramped from −140 to +100 mV, producing practically no changes in the calculated value of $C_m(V)$. *Bottom*, The mean quadratic difference of three model circuit measurements, taken at C_m = 10, 20, or 30 pF, from their expected capacitance values plotted against the ratio of the membrane resistance R_m to the total resistance $R_t = R_a + R_m$. Notice the rapid increase of the quadratic error for $R_m/R_t < 0.5$. *C,* Sample *traces* showing the membrane potential ramp (*top*) that produced the changes of membrane capacitance (*middle*) and OHC length (*bottom*). *D,* Voltage dependence of membrane capacitance (in pF; *circles*, *left y*-axis) and motile responses (in percent units of the cell resting length; *triangles*, *right y*-axis), obtained from the data in *C*. The *sigmoidal curve* through the motility data is a least-square fit obtained from a Boltzmann function with the following parameters: ΔL_{max} = 1.4%, V_p = −20.5 mV, and W = 27.9 mV. The *bell-shaped curve* through the capacitance data is the derivative of the Boltzmann function with the following parameters: C_{max} = 24.3 pF, C_0 = 18.7 pF, V_p = −22.3 mV, and W = 24.3 mV. *Vertical lines* indicate V_p values. *E,* Specific OHC membrane capacitance versus membrane potential measured with standard intracellular and extracellular media (*closed circles*) and with ion channel blockers (*open circles*; see Materials and Methods). Data from two representative cells were fitted by the scaled derivatives of Boltzmann functions with the following parameters: χ_{max} = 1.6 μF/cm^2, V_p = −41.4 mV, and W = 25.5 mV; and χ_{max} = 1.5 μF/cm^2, V_p = −35.3 mV, and W = 25.9 mV, respectively. *Inset,* Representative *I–V curves* obtained with the standard intracellular and extracellular media (*closed circles*) and with ion channel blockers (*open circles*). The residual voltage-independent leakage conductance was not subtracted.

with the overall surface area of the cell. However, the nonlinear voltage-dependent fraction of the cell capacitance is proportional to the area of the lateral membrane surface, where the putative motor elements are located (Huang and Santos-Sacchi, 1993). Therefore, to compare the data obtained from different cells, the nonlinear voltage-dependent capacitance was divided by the area of the lateral plasma membrane as follows:

$$\chi_m(V) = (C_m(V) - C_0)/[(C_0 - C_{ap} - C_{bas})/\chi_{lb}],$$

where $\chi_m(V)$ is the specific nonlinear voltage-dependent capacitance of the lateral plasma membrane (in μF/cm^2). C_{ap} = 4.38 pF and C_{bas} = 1.85 pF are the capacitances of the apical and basal parts of OHC devoid of motor proteins (Huang and Santos-Sacchi, 1993). Therefore, $C_0 - C_{ap} - C_{bas}$ gives the linear voltage-independent capacitance of the lateral plasma membrane. χ_{lb} = 1 μF/cm^2 is the specific capacitance of a lipid bilayer.

Motility measurements. Motility measurements were performed as described in Frolenkov et al. (1997). Briefly OHC movements were recorded with a video camera interfacing with an inverted microscope equipped with differential interference contrast optics to an optical disk recorder (Panasonic TQ-3031F). Digitized images were analyzed off-line with the image-processing system Image 1 (Universal Imaging, West Chester, PA). For movement quantification, a measuring rectangle ranging in length from 5 to 20 μm and composed of 3–15 rows of pixels was positioned across the moving edge of the cell. The average intensity profile across the edge of the cell was calculated, and the number of points in the profile was increased 10 times by cubic spline interpolation. Movement of the cell edge was calculated from the frame-by-frame shift (computed by a least-square procedure) in the interpolated intensity profiles. The sensitivity of the measurement was ~0.02 μm, as determined previously (Frolenkov et al., 1997). Data obtained in this way were fitted by the scaled Boltzmann function:

$$\frac{\Delta L}{L_0}(V) = A_0 - \frac{\Delta L_{max}}{L_0}\frac{1}{1 + \exp(-(V - V_p)/W)}.$$

Here L_0 is the length of the cell at the holding potential V_h, whereas ΔL_{max} is the maximum voltage-dependent length change. V_p and W have the same meaning as in the nonlinear capacitance expression, and A_0 is a suitable constant, such that $\Delta L(V_h) = 0$.

Recording of intracellular [Ca^{2+}] changes. Light from a 175 W stabilized xenon arc source (Lambda DG-4; Sutter Instruments) was coupled via a liquid light guide to the epifluorescence section of an Axiomat microscope (Carl Zeiss, Jena, Germany), which was equipped with an Omega Optical XF100 filter block optimized for the Ca^{2+}-selective dye Oregon Green 488 BAPTA-1. The illumination intensity was attenuated with a neutral density filter to avoid phototoxicity by reducing dye photo-bleaching rates to ≤ 0.1%/sec. Fluorescence images were formed on a scientific grade cooled CCD sensor (Micromax 1300Y; Princeton Instruments, Trenton, NJ) using an oil-immersion objective [100×; numerical aperture (NA) = 1.40; PlanApo; Carl Zeiss]. The sensor's output was binned 3 × 3 and digitized at 12 bits/pixel to produce images that were recorded to a host personal computer controlled by the Axon Imaging Workbench 2.2 software (Axon Instruments) and analyzed off-line. For each image pixel, fluorescence signals were computed as ratios $\Delta F/F = [F(t) - F(0)]/F(0)$, where t is time, $F(t)$ is the fluorescence after a stimulus that causes Ca^{2+} elevation within the cell, and $F(0)$ is the prestimulus fluorescence computed by averaging 10–20 images.

Immunofluorescence. For immunofluorescence, guinea pig cochleae (n = 12) were opened and fixed in 4% paraformaldehyde in PBS, pH 7.4, for 1 hr. Samples were permeabilized with 0.5% Triton X-100 in PBS for 30 min, followed by overnight incubation in blocking solution (5% goat serum plus 2% bovine serum albumin in PBS). Samples were incubated for 1 hr with 2.5 μg/ml affinity-purified primary antibody: the anti-Ca^{2+}/calmodulin-dependent protein kinase IV (CaMK-IV) antibody (Santa Cruz Biotechnology, Santa Cruz, CA) or the anti-IP_3 receptor antibody (Calbiochem). As a secondary antibody, we used the FITC-conjugate anti-rabbit IgG (Amersham, Piscataway, NJ). Samples were viewed with a Zeiss laser scanning confocal microscope or a Zeiss Axiophot microscope equipped with a 63× objective (NA = 1.4). No signal was detected using the

secondary antibody alone. For the CaMK-IV labeling, we also performed an additional control, in which the primary antibody was preadsorbed for 1 hr at room temperature with an excess of the immunogenic peptide (50 μg/ml), which suppressed the labeling.

RESULTS

Validation of the recording procedure

It is a common practice to block at least the most prominent K^+ membrane conductance to facilitate the investigation of the electromotility-associated charge movement and/or voltage-dependent OHC capacitance (see Santos-Sacchi, 1991; Gale and Ashmore, 1997). Unfortunately, this approach cannot be applied to the study of the effects of ACh on the OHC voltage-dependent capacitance because the Ca^{2+}-activated outward K^+ current is the main indicator of the successful activation of OHC ACh receptors. Therefore, it was necessary to develop a procedure for the simultaneous measurement of C_m and cell motility (ΔL) under conditions of varying R_m. When the ratio of R_m to R_t (see Materials and Methods) was > 0.6, the error affecting our capacitance measurements was $< 16\%$ (Fig. 1*B*). This allowed us to determine the voltage dependence of motility and capacitance from the same voltage ramp applied to the cell membrane under whole-cell patch-clamp recording conditions (Fig. 1*C*). The OHC nonlinear capacitance followed the derivative of the motile response (Fig. 1*D*), as described previously (Santos-Sacchi, 1991). The differences between the Boltzmann parameters used to fit motility and capacitance data—the midpoint potential (V_p) and the potential sensitivity (W) (see Materials and Methods)—were not statistically significant at the $p = 0.05$ level for $n = 14$ control cells.

As a control, we measured also the voltage dependence of OHC capacitance in a different set of cells using intracellular and extracellular solutions designed to block the majority of ionic membrane conductances (see Materials and Methods). The values of V_p, W, and the maximum specific capacitance χ_{max} were -18 ± 4 mV, 33 ± 1 mV, and 2.1 ± 0.2 μF/cm^2 ($n = 10$) for normal and -30 ± 9 mV, 36 ± 2 mV, and 2.0 ± 0.1 μF/cm^2 ($n = 20$) for blocking solutions, respectively. No statistically significant differences between the two groups were found ($p > 0.05$; Fig. 1*E*, two sample *curves* shown). These parameter values are in agreement with previous reports (see Santos-Sacchi, 1991). Two samples of current–voltage (*I–V*) relationships, obtained from each group by subjecting the membrane potential to a ramp, are plotted in the Figure 1*E, inset*. With blocking solutions, the whole-cell current was mainly caused by a voltage-independent leakage conductance that reversed near 0 mV.

Our measurements of C_m were robust relative to the changes of R_m not only in a model electrical circuit (Fig. 1*B*) but also in real cells, provided that the value of R_m/R_t was sufficiently high. Figure 2 illustrates an experiment in which the electrically evoked OHC movements partly destroyed the seal between pipette and membrane, resulting in the development of a leak. After the voltage ramps, the apparent R_m fell from ~60 to 6 MΩ, changing the R_m/R_t ratio from 10 to 0.5. In spite of such dramatic changes, our system satisfactorily tracked the capacitance of the cell.

Nevertheless, we were unable to measure C_m in short OHCs (<30 μm), in which a large inward current was activated at potentials more positive than -20 mV, resulting in a dramatic drop of R_m below the value of R_a. Because capacitance could not be reliably measured under such unfavorable conditions, these cells have not been included in the results. This was an unfortunate limitation, because the largest ACh-evoked currents were found in such short cells from the high-frequency end of the cochlea (see also Housley and Ashmore, 1991).

Effect of ACh on the OHC voltage-dependent capacitance and electromotility

Focal applications of ACh (100 μM) to the synaptic pole of the OHC, held at approximately $V_h = -60$ mV ($n = 10$), elicited outward currents of 50–200 pA and simultaneous 5–40% drops in R_m (Fig. 3*A*). The latency of this outward current was in the range of 150–250 msec (Fig. 3*B*), i.e., much longer than the drug delivery time that was estimated on the order of 20 msec, on the basis of similar experiments in which salicylate was applied to elicit a rapid decrease in the OHC nonlinear capacitance (Tunstall et al., 1995) (G. I. Frolenkov, unpublished results). In two experiments, a small inward current preceded the ACh-evoked outward current (Fig. 3*B*). The voltage dependence of the latter (Fig. 3*D*) had a characteristic N shape (Blanchet et al., 1996; Evans, 1996). These data agree with the view that ACh activates a small inward current, partly carried by Ca^{2+}, which in turn triggers a large Ca^{2+}-activated outward K^+ current (Evans, 1996). Application of apamin (1 μM) to the bath suppressed the ACh-evoked outward current (data not shown), indicating that it was carried through small-conductance Ca^{2+}-activated K^+ channels (Blatz and Magleby, 1986; Yamamoto et al., 1997).

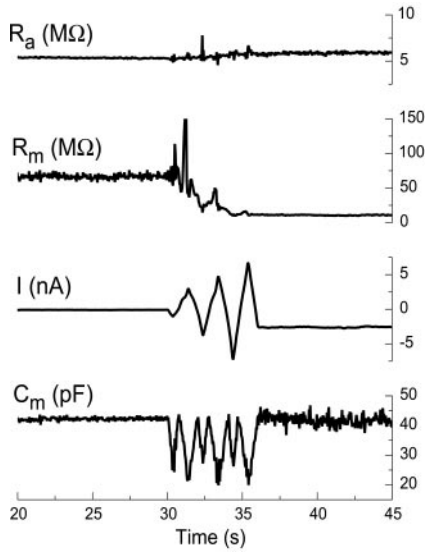

Figure 2. Stability test for capacitance measurements. Because of variations of the whole-cell recording conditions, the calculated value of membrane resistance decreased ~10 times after the voltage ramp stimulation. *Traces* show the simultaneous measurements of the following parameters (from *top* to *bottom*): R_a, access resistance; R_m, membrane resistance; *I*, whole-cell current; and C_m, membrane capacitance.

In spite of the prominent ACh-induced current responses, we observed virtually no ACh-induced changes in the OHC voltage-dependent membrane capacitance (Fig. 3*A,E,F*). However, simultaneous measurements of the length changes of the same cell showed a significant ACh-induced increase of the electromotile responses (Fig. 4). In a group of cells showing a well preserved cylindrical cell body ($n = 4$), which we took as an indication of normal turgor condition, the electromotile responses increased by 2–26% after ACh, without statistically significant changes (at $p = 0.05$ level) in the peak value of $C_m(V)$. After ACh, the midpoint of the voltage sensitivity of the membrane capacitance shifted slightly toward more hyperpolarized values ($\Delta V_p = -3.9 \pm 0.8$ mV; $p < 0.05$). The ACh-induced stationary elongation of the cells of this group ($\Delta L = 2.4 \pm 3.0\%$) was not statistically significant ($p = 0.48$).

Cell turgor (intracellular pressure) is an important factor in the control of OHC electromotility (Shehata et al., 1991; Chertoff and Brownell, 1994) and nonlinear capacitance (Iwasa, 1993; Kakehata and Santos-Sacchi, 1995). Therefore, it was possible that the increase of electromotility after ACh depended on turgor increase, with turgor and ACh effects canceling each other at the level of the nonlinear capacitance. To exclude this possibility, we tested the effect of ACh on OHCs ($n = 4$) whose natural turgor had been removed by applying negative pressure to the patch pipette (see Kakehata and Santos-Sacchi, 1996; Santos-Sacchi and Huang, 1998). ACh did not change the maximal voltage-dependent capacitance of these collapsed OHCs but shifted slightly the peak of $C_m(V)$ ($\Delta V_p = -3.3 \pm 1.2$ mV; $p < 0.05$).

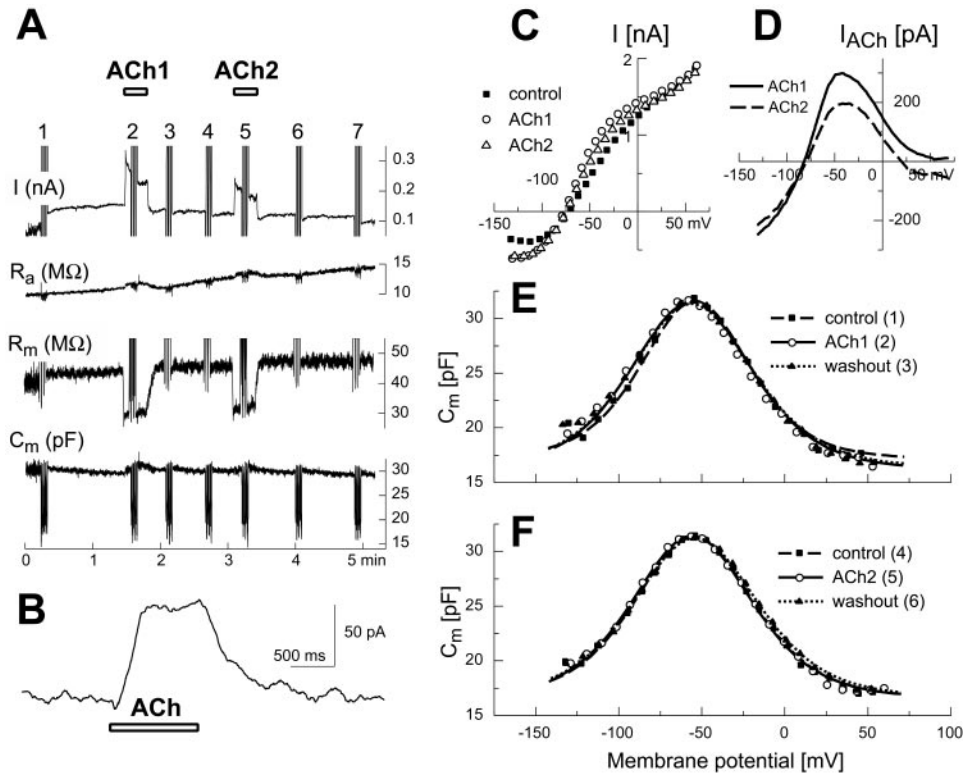

Figure 3. Acetylcholine does not affect OHC capacitance. *A,* Monitoring cell parameters before, during, and after two consecutive applications of ACh (100 μM; 20 sec; *open horizontal bars*). From *top* to *bottom,* the following parameters were measured: *I*, whole-cell current; R_a, access resistance; R_m, membrane resistance; and C_m, membrane capacitance. *Trace deflections* are caused by the delivery of triangular voltage ramps to the cell (see Fig. 1*C*; ramps are *numbered 1–7*). *B,* Sample of the current response to ACh (100 μM; 1 sec) from a different cell, shown on a faster time scale to reveal a barely noticeable inward current preceding the large outward current. *C,* Current–voltage *I–V* relationship without ACh (*control*; *closed squares*; average of the data from ramps 1, 3, 4, 6, and 7) and during the first (*ACh1*; *open circles*) and the second (*ACh2*; *open triangles*) application of ACh in *A*. *D,* ACh-sensitive fraction of the *I–V curve*, obtained by subtraction of the whole-cell current during ACh application from the mean of the whole-cell currents before and after ACh (data from *C*). *E, F*, Insensitivity of the capacitance–voltage $C_m(V)$ relationship to ACh, measured before (*control*; *closed squares*), during (*open circles*), and after (*washout*; *closed triangles*) the first (*E*) and the second (*F*) application of ACh (*ACh1, ACh2* in *A*). $C_m(V)$ relationships were obtained from ramps *1–6* (indicated in *parentheses*). Data were fitted by the scaled derivatives of Boltzmann functions. All data points were obtained at $R_m/R_t < 0.7$; therefore the estimated error of C_m measurements was < 2 pF.

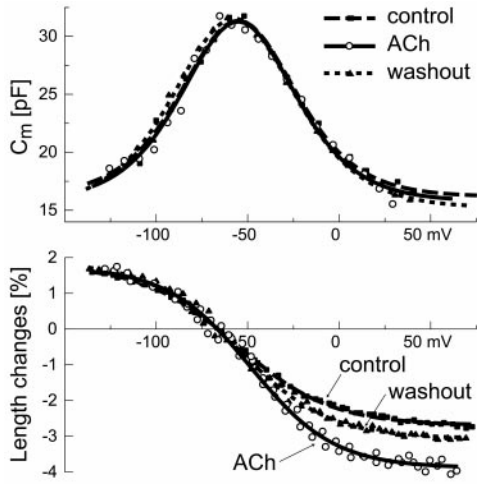

Figure 4. Functional decoupling of electromotility and nonlinear capacitance after ACh application. Capacitance–voltage relationships $C_m(V)$ (*top*) and the voltage dependence of electromotile responses $\Delta L(V)$ (*bottom*), measured before (*control*; *closed squares*), during (*ACh*; *open circles*), and after (*washout*; *closed triangles*) ACh application. Data are from the same experiment shown in Figure 3, *A* and *C–F*. Capacitance data were fitted by the scaled derivative of Boltzmann functions with the following parameters: C_{max} = 15 pF, C_0 = 16 pF, V_p = −55 mV, and W = 21 mV (*control*); C_{max} = 15 pF, C_0 = 16 pF, V_p = −50 mV, and W = 21 mV (*ACh*); and C_{max} = 16 pF, C_0 = 15 pF, V_p = −57 mV, and W = 22 mV (*washout*). Motility data were fitted by the Boltzmann functions with the following parameters: ΔL_{max} = 4.5%, V_p = −56 mV, and W = 25 mV (*control*); ΔL_{max} = 5.6%, V_p = −52 mV, and W = 23 mV (*ACh*); and ΔL_{max} = 4.9%, V_p = −58 mV, and W = 24 mV (*washout*).

Effect of ionomycin

To determine whether the elevation of $[Ca^{2+}]_i$ affects the OHC nonlinear capacitance, we applied the Ca^{2+} ionophore ionomycin. This drug is known to induce a generalized, transient increase of $[Ca^{2+}]_i$ by making the plasma membrane, as well as the membranes of intracellular Ca^{2+} stores, permeable to Ca^{2+} (Liu and Hermann, 1978; Smith et al., 1989).

Puff applications of ionomycin (25 μM; 20 sec) produced dramatic increases of $[Ca^{2+}]_i$ in OHCs ($\Delta F/F$ = 84 ± 28%; n = 10), widespread along the whole-cell body (Fig. 5*A–C*). The $[Ca^{2+}]_i$ increase was accompanied by a voltage-independent elongation of the cell (Fig. 5*C*, *middle*) amounting, on average, to $\Delta L/L_0$ = 4.6 ± 0.9% (n = 10; $p < 0.001$). In 70% of the cells this elongation was terminated by the loss of cell turgor, either temporary or permanent. Usually, the $[Ca^{2+}]_i$ initially elevated by ionomycin showed a very slow decline, and it did not return to the baseline within 10–20 min. Further applications of ionomycin to the same cell produced additional step-like increases of $[Ca^{2+}]_i$, up to the saturating level of the fluorescent indicator. Saturation was commonly reached after the second or third application. Only data from the first applications are reported here.

Similar to ACh, ionomycin was able to evoke a transient outward current in 50% of the cells (range, 15–320 pA; n = 6) at V_h = −50 mV (Fig. 5*C*, *bottom*). The voltage dependence of this current had an N shape (Fig. 5*E*, *inset*) similar to that of the ACh-induced outward current (compare Fig. 3*D*). The simplest explanation is that ionomycin evoked Ca^{2+}-activated K^+ current. At the concentration of 10 μM, ionomycin evoked only an outward current in three out of seven cells tested. In the remainder of the cells, no current response was detected, although an increase of $[Ca^{2+}]_i$ was always observed. At the higher concentration (25 μM), in four out of nine cells the outward current was followed by an inward current with a reversal potential close to zero (data not shown). Such inward current was generally found in cells with a high basal level of $[Ca^{2+}]_i$, as judged by the resting fluorescence level of the cell and by the relatively small difference between resting and saturating fluorescence. Ca^{2+}-activated nonselective cation channels, possibly underlying the observed inward currents, have been described in OHCs (Van den Abbeele et al., 1996). The nature of this second current was not investigated further.

Usually, we did not observe any substantial changes of OHC voltage-dependent capacitance after ionomycin application, except at a relatively high drug concentration (50 μM) or with repeated applications of the drug to cells whose resting $[Ca^{2+}]_i$ level was initially already high (data not shown). In cells with low resting

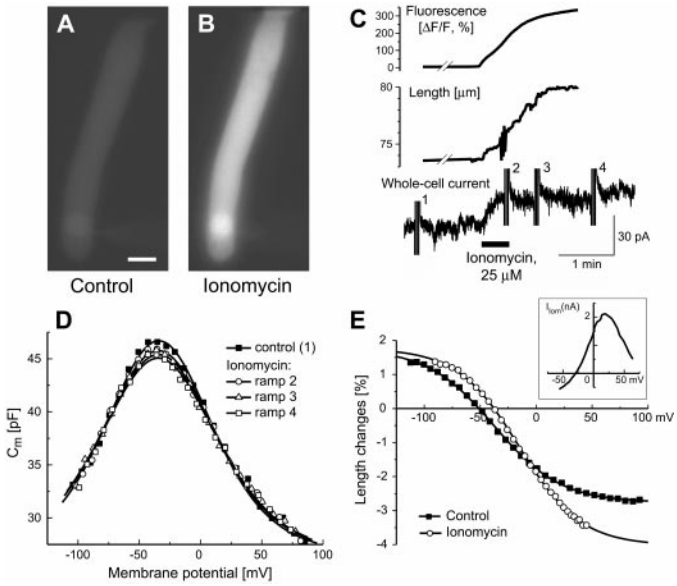

Figure 5. Ionophore-mediated elevation of intracellular free Ca^{2+} concentration increases the OHC resting length, enhances electromotile responses, but does not affect nonlinear capacitance. *A,* Fluorescent image of an OHC filled with Oregon Green 488 BAPTA-1 (50 μM) through the patch pipette. *B,* The same cell shown in *A* 1 min after the application of 25 μM ionomycin. Scale bar, 10 μm. *C,* Time course of fluorescence changes (*top*), resting length (*middle*), and whole-cell current (*bottom*) after application of ionomycin to the cell shown in *A* and *B*. Fluorescence intensity was computed by averaging pixel values throughout the cell body. *Deflections* on the current and length records are caused by the delivery of triangular voltage ramps (*numbered 1–4*) to the cell. A *closed horizontal bar* at the *bottom* of the *panel* indicates the timing of the drug application. *D,* Membrane capacitance–voltage $C_m(V)$ relationships before (*control*; ramp 1; *closed squares*) and after (*ramps 2, 3, 4*; *open symbols*) application of ionomycin, obtained during the correspondingly numbered voltage ramps in *C*. Data were fitted by the scaled derivatives of the Boltzmann function. *E,* Electromotility responses of a different OHC before application of ionomycin (*Control*; *closed squares*) and after recovery from ionomycin-induced turgor loss (*Ionomycin*, *open circles*; 2 min after drug application). Data were fitted by Boltzmann functions. *Inset,* A sample of the current–voltage relationship of the ionomycin-sensitive fraction of the whole-cell current.

$[Ca^{2+}]_i$, ionomycin produced virtually no changes of the cell nonlinear capacitance, even at a concentration of 25 μM (Fig. 5*D*).

Three cells were observed in bright field to investigate electromotile responses before and after the application of ionomycin (25 μM). In all three cases the maximum voltage-activated motile responses of the OHCs increased (Fig. 5*E*) by 0.73, 0.63, and 1.24% of the cell length [0.87 ± 0.19% (mean ± SE); $p < 0.05$].

Effect of ACh and ionomycin on OHCs under perforated-patch conditions

Metabotropic effects of ACh may be significantly compromised under conventional whole-cell patch-clamp recording conditions because of washout of intracellular constituents during the first minutes after breaching the membrane patch (Horn and Marty, 1988). Therefore, we investigated the effects of ACh and ionomycin on the cell's membrane capacitance under perforated-patch conditions, i.e., when the membrane patch at the pipette tip was not physically broken but was made permeable to small ions with nystatin (Horn and Marty, 1988). Under these conditions, we managed to measure reliably the OHC capacitance only in the two experiments shown in Figure 6. Neither ACh (Fig. 6*A*; 100 μM; 20 sec) nor ionomycin (Fig. 6*B*; 25 μM; 20 sec) produced measurable changes of C_m in these experiments.

Modulation of the operating range of OHC electromotility by protein phosphorylation

It has been suggested that the effect of ACh on OHC electromotility is mediated by a Ca^{2+}-dependent phosphorylation of cytoskeletal proteins (Dallos et al., 1997). We tested whether phosphorylation affects also the voltage sensor of the OHC motor by investigating the effects of inhibitors and promoters of protein phosphorylation on $\chi_m(V)$. Cells were preincubated at 37°C in okadaic acid, a powerful inhibitor of protein phosphatase-1 and -2A that promote phosphorylation of a wide range of proteins *in vivo* (Haystead et al., 1989), and the specific calmodulin inhibitors trifluoperazine and W-7. After incubation, the cytoplasmic morphology of the cells in the dish did not change visibly. A significant number of OHCs remained viable according to our selection criteria (see Materials and Methods). After incubation in okadaic acid (1 μm; 30–60 min), $\chi_m(V)$ shifted in the hyperpolarized direction (Fig. 7, *top*). Incubation for 30–60 min with trifluoperazine (30 μM) and W-7 (150 μM) shifted $\chi_m(V)$ in the opposite direction (Fig. 7, *top*). The voltage dependence of the electromotile responses, $\Delta L(V)$, was affected similarly (Fig. 7, *middle*). The effects of these reagents on $\chi_m(V)$ did not depend on intracellular pressure because they were reproducible both in artificially collapsed cells and in cells with apparently normal turgor. In artificially collapsed OHCs we observed the following values of the potential at the peak of $\chi_m(V)$: −37.7 ± 3.1 mV (control; $n = 9$), −56.8 ± 5.2 mV (okadaic acid; $n = 4$), −2.2 ± 1.9 mV (trifluoperazine; $n = 3$), and 0.9 ± 1.2 mV (W-7; $n = 3$). Parameters of $\chi_m(V)$ and $\Delta L(V)$ relationships for OHCs with apparently normal turgor are shown in Table 1. Comparing the effects of these reagents (Fig. 7) with those produced by ACh (Fig. 3) indicates that the shift of $\chi_m(V)$ induced by ACh is only ~5–6% of the maximal range covered by phosphorylation.

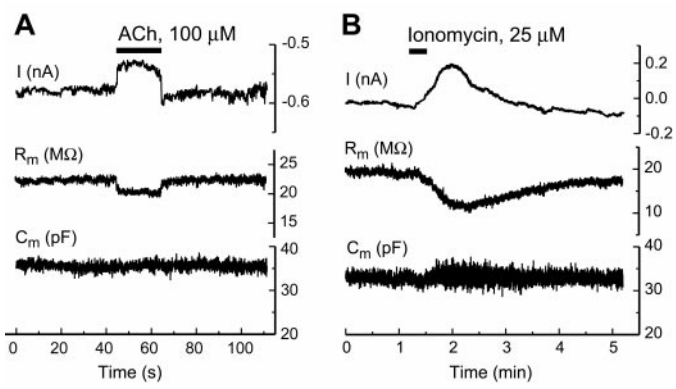

Figure 6. ACh (*A*) and ionomycin (*B*) do not affect the OHC capacitance even under perforated-patch conditions. From *top* to *bottom*, the following parameters were measured: *I*, whole-cell current, R_m, membrane resistance; and C_m, membrane capacitance. The *closed horizontal bars* at the *top* of *A* and *B* indicate the timing of drug application.

The reagents tested did not change significantly the maximal nonlinear capacitance χ_{max}, the maximal motile response ΔL_{max}, or the voltage sensitivity W of capacitance and electromotility, with the exception of okadaic acid that changed the voltage sensitivity W of $\chi_m(V)$ (Table 1). However, they increased the zero-current voltage (Fig. 7, *bottom*), probably because of the disruption of mechanisms responsible for maintaining the intracellular potential (Hasin and Barry, 1984).

It is well known that isolated OHCs are depolarized (Ashmore, 1987). Immediately after achieving the whole-cell configuration, the zero-current potential V_z is rarely more negative than −30 mV and gradually shifts to more hyperpolarized values over 3–5 min as potassium in the patch pipette equilibrates with the cell interior. This explains the difference in the values of V_z in Figures 3*C* and 7, *bottom*. The latter were obtained within 60 sec after breaching the patch of membrane under the recording pipette to minimize the dialysis of the intracellular constituents with the pipette solution. The −6 mV shift in V_z reported for long OHCs in the presence of okadaic acid (Jagger and Ashmore, 1999) is not compatible with data in Figure 7 simply because the latter were not obtained in steady-state conditions.

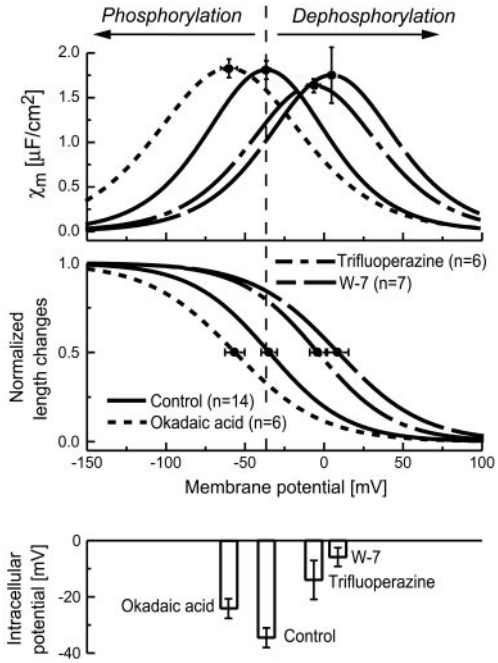

Figure 7. Modulation of the electromotility operating range by protein phosphorylation. *Top,* The voltage-dependent nonlinear capacitance shifts to hyperpolarizing potentials after preincubation of OHCs with okadaic acid (1 μM), a nonspecific inhibitor of native phosphatases. Preincubation with agents inhibiting Ca^{2+}/calmodulin-dependent phosphorylation (trifluoperazine, 30 μM; W-7, 150 μM) shifts the *curve* in the opposite direction. Each *curve* is the average of measurements from several cells ($n > 5$) fitted by the derivative of Boltzmann functions, with the SE for both voltage and capacitance plotted at the maximum of each *curve*. *Middle*, Corresponding shifts of the motile responses. To highlight the shift of the *midpoint* of the *curves*, the maximal motile responses were normalized to 1. The parameter ΔL_{max} varied substantially between the groups of cells, but the differences were not statistically significant. Boltzmann parameters for the *curves* are given in Table 1. *Bottom,* Effects of these reagents on the zero-current potentials measured from the corresponding *I–V curves*.

Immunohistochemical localization of Ca^{2+} release channels and CaMK-IV

Ca^{2+}/calmodulin-dependent protein phosphorylation often involves the release of Ca^{2+} from IP_3-gated intracellular stores (Berridge, 1993). To determine whether the key elements of this pathway colocalize with the electromotile apparatus, we immunolabeled whole-mount preparations of the organ of Corti with fluorescent antibodies raised against IP_3 receptors (Fig. 8, *left*) and CaMK-IV (Fig. 8, *right*). Labeling for both the IP_3 receptors and CaMK-IV was found to be concentrated at the cell cortex, along the OHC lateral wall between the nucleus and the cuticular plate. The lateral plasma membrane of the OHC contains the putative molecular motors (Dallos et al., 1991; Kalinec et al., 1992) and is underlined by a cortical cytoskeleton adjacent to layers of endoplasmic reticulum named lateral cisternae (Holley et al., 1992). The thicker pattern of labeling was observed for the IP_3 receptor localization (Fig. 8, *left*), suggesting that it is associated with the lateral cisternae. The thinner labeling observed for the CaMK-IV (Fig. 8, *right*) suggests association with the cortical cytoskeleton or the plasma membrane. Some punctuated labeling was also observed below the cuticular plate and at the synaptic pole of the OHC, for both the IP_3 receptor and the CaMK-IV.

DISCUSSION

Our results show, for the first time, that the voltage sensitivity of the OHC electromotile mechanism can be modulated by reagents affecting Ca^{2+}/calmodulin-dependent phosphorylation. Inhibition of protein phosphorylation produces a depolarizing shift of voltage sensitivity, whereas activation leads to a hyperpolarizing shift (Fig. 7). The invariance of the capacitance measurement in the presence and in the absence of ion channel blockers (Fig. 1*E*) argues against the possibility that the effects of phosphorylation are indirect effects on ion channels that in turn affect the motors. Calcium currents in OHCs are extremely small, and none of the several Ca^{2+} channel blockers we tested (Frolenkov et al., 1998a) had any effect on OHC electromotility. Therefore, it seems unlikely that the observed effects may be caused by modification of calcium influx produced by the phosphorylation/dephosphorylation of calcium channels. These effects are also not related to the changes of cell turgor, because they were present in artificially collapsed cells as well as in cells with apparently normal turgor.

We have measured the voltage dependence of the nonlinear membrane capacitance $C_m(V)$ and length change $\Delta L(V)$ in isolated OHCs without blocking ion channels. In these cells, most ion channels are localized to a fraction of the plasma membrane near the synaptic pole (Santos-Sacchi et al., 1997), where their density is several fold lower than the density of the putative motor proteins in the basolateral membrane [up to $6000/\mu m^2$ (Frolenkov et al., 1998a)]. On the basis of our own measurement of the total motor's charge density movement:

$$\int_{-\infty}^{+\infty} \chi_m(V)\mathrm{d}V,$$

we estimate the number of gating charges per protein to be ~2. This is well outside the range of 10–15 gating charges per potassium channel estimated by Aidley and Stanfield (1996). Because voltage-dependent potassium currents provide by far the dominant contribution to the OHC ionic conductance (Mammano and Ashmore, 1996), we conclude that the charge movement underlying the voltage dependence of $C_m(V)$ does not include a significant contribution from ion channel gating. In support of this conclusion we did not find any significant differences measuring $C_m(V)$ with and without ionic channel blockers (Fig. 1*E*).

Although we were able to detect a small shift of the voltage sensitivity of $C_m(V)$ in the hyperpolarizing direction after ACh, this was at least 10 times smaller than the maximum shift induced by protein phosphorylation. We observed a similar small effect on the OHC nonlinear capacitance after the application of ATP, a second natural ligand capable of promoting an $[Ca^{2+}]_i$ increase in OHCs (Mammano et al., 1999). The application of ACh to isolated OHCs evokes both a fast ionotropic response and a slow metabotropic response. The fast response is a BAPTA-sensitive outward current, attributed to K^+ efflux through Ca^{2+}-activated K^+ channels (Blanchet et al., 1996; Evans, 1996). The slow response is an increase in OHC motile responses, with a delay of ~10 sec, attributed to the activation of a Ca^{2+}-dependent phosphorylation of cytoskeletal proteins and the subsequent decrease in the global axial stiffness of the cell (Dallos et al., 1997). Our results confirm and extend these findings. After the focal application of ACh to the synaptic pole of OHCs, we observed a fast apamin-sensitive outward current (Fig. 3) as well as an increase of the OHC electromotile responses (Fig. 4), independent of any appreciable change in the nonlinear capacitance (Fig. 3).

Changes in intracellular pressure (turgor) are known to shift the midpoint of the voltage sensitivity V_p of $C_m(V)$ by as much as 40 mV (Kakehata and Santos-Sacchi, 1995). In contrast, V_p is relatively insensitive to the variations of intracellular pressure when OHCs are artificially deflated below the point of collapse (Kakehata and Santos-Sacchi, 1995). Under these conditions ACh did not alter $C_m(V)$. Likewise, in cells with apparently normal turgor, the increase in the $\Delta L(V)$ induced by ACh caused no significant change in the concurrently measured $C_m(V)$, both under whole-cell (Fig. 3) and under perforated-patch (Fig. 6) conditions. Therefore we conclude that (1) the effects of ACh on OHC electromotility are not mediated by turgor changes and (2) they do not involve a modulation of the operating range of the motor's voltage sensor.

It has been shown in unclamped OHCs that the increase in the concentration of intracellular Ca^{2+} induced by the selective Ca^{2+}

Table 1. Parameters of $\chi_m(V)$ and $\Delta L(V)$ relationships for the control group of OHCs and the cells preincubated with okadaic acid (1 μM), trifluoperazine (30 μM), and W-7 (150 μM)

	Capacitance measurements				Electromotility measurements		
	χ_{max} ($\mu F/cm^2$)	C_0 (pF)	V_p (mV)	W (mV)	ΔL_{max} (%)	V_p (mV)	W (mV)
Control ($n = 14$)	1.81 ± 0.10	22.9 ± 1.5	-34.8 ± 3.6	26.6 ± 0.8	2.5 ± 0.6	-34.7 ± 5.0	24.6 ± 1.1
Okadaic acid ($n = 6$)	1.82 ± 0.10^N	20.4 ± 1.1^N	$-60.2 \pm 5.2^{***}$	$30.7 \pm 1.7^{***}$	3.2 ± 0.6^N	$-56.5 \pm 6.2^{**}$	27.6 ± 2.0^N
Trifluoperazine ($n = 6$)	1.63 ± 0.07^N	22.9 ± 1.9^N	$-6.5 \pm 4.2^{***}$	27.3 ± 2.4^N	2.4 ± 0.4^N	$-4.0 \pm 5.0^{**}$	24.1 ± 4.1^N
W-7 ($n = 7$)	1.75 ± 0.31^N	25.9 ± 3.4^N	$4.7 \pm 2.3^{***}$	26.9 ± 1.8^N	2.8 ± 1.1^N	$8.7 \pm 6.7^{***}$	26.9 ± 1.8^N

Average values and the corresponding SEs are shown. To minimize the potential adverse effects of dialyzing the intracellular constituents with the pipette solution, measurements were taken within 60 sec after establishing whole-cell recording conditions. Statistical significance of the difference between values of any parameter in control and treated OHCs is designated as follows: N, no statistical significance ($p > 0.05$); $^{**}p < 0.01$; $^{***}p < 0.001$.

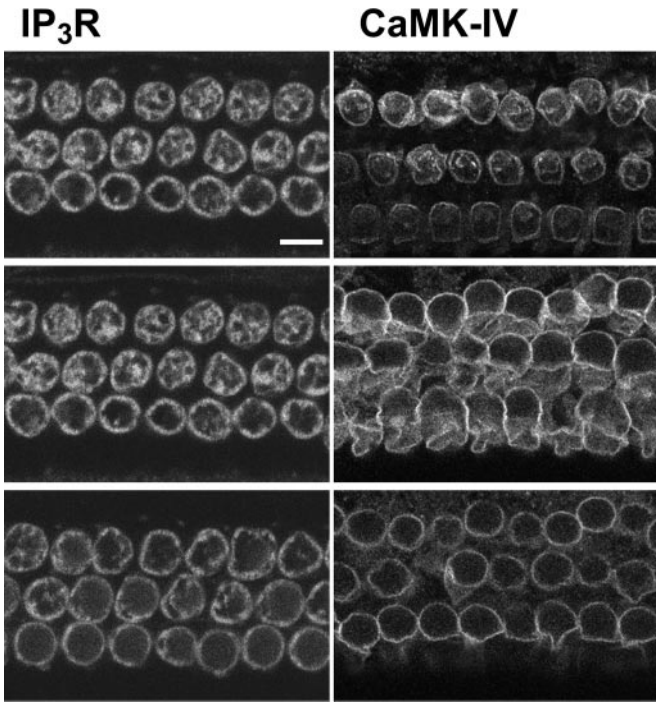

Figure 8. Colocalization of IP_3 receptors (*IP_3R; left*) and CaMK-IV (*right*) to the lateral wall of OHCs by confocal immunofluorescence microscopy. Optical cross sections (0.4 μm) were taken at 20 μm intervals, below the cuticular plate (*top*), halfway down the length of the cells (*middle*), and in the nuclei region (*bottom*). In both cases, the antibodies distinctly labeled the lateral wall of the OHC visualized as annular fluorescence patterns. Scale bar, 10 μm.

ionophore ionomycin is followed by cell elongation promoted by a Ca^{2+}/calmodulin-dependent pathway (Dulon et al., 1990; Coling et al., 1998). In our experiments both ACh and ionomycin evoked outward currents (Figs. 3*A*, 5*C*), most probably because of the opening of Ca^{2+}-activated K^+ channels. Similar to ACh (Fig. 4), ionomycin was able to increase the OHC motile responses without a significant effect on the cell voltage-dependent capacitance (Figs. 4, 5*E*). Thus the effect of ACh on the electromotility is not unique; in both cases the crucial steps seem to involve the elevation of $[Ca^{2+}]_i$.

In unclamped OHC an outward current would produce hyperpolarization and consequently an electrically evoked elongation of the cell. In our experiments, OHCs were voltage-clamped, and their elongation after ionomycin should be attributed to some mechanism changing the mechanical properties of the cell. We conclude that the ionomycin-induced elongation of the OHC (Fig. 5*C*) is likely to be a passive reaction of a turgid cell to a decrease of its axial stiffness, resulting from a Ca^{2+}-dependent modification of cytoskeletal proteins. This mechanism was proposed by Dallos et al. (1997) to explain the increase of the electromotile responses induced by ACh.

Using immunofluorescence, we determined, in agreement with others (Koyama et al., 1999), that some key elements required to activate a Ca^{2+}-dependent protein phosphorylation cascade, i.e., IP_3 receptors and CaMK-IV, are present along the OHC lateral wall (Fig. 8) where the putative molecular motors of the OHC are localized (Dallos et al., 1991; Kalinec et al., 1992). Like the cortical lattice in erythrocytes, the filamentous network of OHC cytoskeletal proteins seems to be anchored to the plasma membrane by periodic protein pillars ~25 nm long (Raphael and Wroblewski, 1986). Normally, the relatively stiff circumferential filaments may restrain large changes in cell diameter, whereas the elastic cross-links offer less resistance. The cortical lattice is a highly orthotropic structure because its resultant circumferential stiffness modulus is approximately one order of magnitude larger than the axial one (Tolomeo et al., 1996). Consequently, a major function of the cytoskeleton would be to direct electrically driven shape changes along the longitudinal axis of the cell (Tolomeo et al., 1996). A system of flattened, membrane-bound intracellular compartments, the subsurface cisternae (Engstrom, 1958), is found near the cytoskeletal lattice. Closely related is the synaptic cisterna, located at the basal (synaptic) pole of the cell. Together with the cytoskeletal lattice and plasma membrane, they form a complex structure, the cell cortex (Holley et al., 1992). The preferential distribution of Ca^{2+}-ATPase near the innermost layer of the cisternae, in strict apposition to linearly arranged mitochondria, supports a role for these structures as intracellular Ca^{2+} stores (Schulte, 1993), a conclusion compatible with our present immunofluorescence data. Release of Ca^{2+} from these putative stores may activate biochemical cascades that modulate the cell's axial stiffness and the voltage sensitivity of the plasma membrane motors.

In conclusion, our data suggest that the OHC motor output may be affected by two Ca^{2+}-dependent pathways. One pathway targets the proteins of the cortical cytoskeleton, altering the global axial stiffness of the cell. The other pathway targets the putative membrane motors, shifting its operating range. Our results show that the natural ligands ACh (Figs. 3, 4, 6) and ATP (Mammano et al., 1999) do not cause changes in the voltage sensitivity of the membrane motors in isolated OHCs maintained at room temperature and under whole-cell patch-clamp recording conditions. However, there are strong indications for the existence of functional intracellular Ca^{2+} stores in close proximity to the OHC electromotile machinery. Release of Ca^{2+} from such stores may potentially modulate the function of the OHC motors very effectively. It remains to be determined what sort of physiological stimuli may be responsible for the activation of these putative Ca^{2+} release-dependent cascades.

REFERENCES

Aidley DJ, Stanfield PR (1996) Ion channels: molecules in action, pp 180–184. Cambridge, UK: Cambridge UP.

Ashmore JF (1987) A fast motile response in guinea-pig outer hair cells: the cellular basis of the cochlear amplifier. J Physiol (Lond) 388:323–347.

Berridge MJ (1993) Inositol triphosphate and calcium signaling. Nature 361:315–325.

Blanchet C, Erostegui C, Sugasawa M, Dulon D (1996) Acetylcholine-induced potassium current of guinea pig outer hair cells: its dependence

on a calcium influx through nicotinic-like receptors. J Neurosci 16:2574–2584.
Blatz AL, Magleby KL (1986) Single apamin-blocked Ca-activated K^+ channels of small conductance in cultured rat skeletal muscle. Nature 323:718–720.
Chertoff ME, Brownell WE (1994) Characterization of cochlear outer hair cell turgor. Am J Physiol 266:C467–C479.
Coling DE, Bartolami S, Rhee D, Neelands T (1998) Inhibition of calcium-dependent motility of cochlear outer hair cells by the protein kinase inhibitor, ML-9. Hear Res 115:175–183.
Dallos P (1992) The active cochlea. J Neurosci 12:4575–4585.
Dallos P, Evans BN, Hallworth R (1991) Nature of the motor element in electrokinetic shape changes of cochlear outer hair cells. Nature 350:155–157.
Dallos P, He DZZ, Sziklai I, Metha S, Evans BN (1997) Acetylcholine, outer hair cell electromotility, and the cochlear amplifier. J Neurosci 17:2212–2226.
Doi T, Ohmori H (1993) Acetylcholine increases intracellular Ca^{2+} concentration and hyperpolarizes the guinea-pig outer hair cell. Hear Res 67:179–188.
Dulon D, Zajic G, Schacht J (1990) Increasing intracellular free calcium induces circumferential contractions in isolated cochlear outer hair cells. J Neurosci 10:1388–1397.
Elgoyhen AB, Johnson DS, Boulter J, Vetter DE, Heinemann S (1994) Alpha 9: an acetylcholine receptor with novel pharmacological properties expressed in rat cochlear hair cells. Cell 79:705–715.
Engstrom H (1958) Structure and innervation of the inner ear sensory epithelia. Int Rev Cytol 7:535–585.
Evans MG (1996) Acetylcholine activates two currents in guinea-pig outer hair cells. J Physiol (Lond) 491:563–578.
Eybalin M (1993) Neurotransmitters and neuromodulators of the mammalian cochlea. Physiol Rev 73:309–373.
Frolenkov GI, Kalinec F, Tavartkiladze GA, Kachar B (1997) Cochlear outer hair cell bending in an external electric field. Biophys J 73:1665–1672.
Frolenkov GI, Atzori M, Kalinec F, Mammano F, Kachar B (1998a) The membrane-based mechanism of cell motility in cochlear outer hair cells. Mol Biol Cell 9:1961–1968.
Frolenkov GI, Belyantseva IA, Kachar B (1998b) Electromotility influences the axial stiffness of the outer hair cells. In: Abstracts of 21st meeting of the Association for Research in Otolaryngology (Popelka GR, ed), abstract 254. St. Petersburg Beach, FL: Association for Research in Otolaryngology.
Gale JE, Ashmore JF (1997) The outer hair cell motor in membrane patches. Pflügers Arch 434:267–271.
Hasin Y, Barry WH (1984) Myocardial metabolic inhibition and membrane potential, contraction, and potassium uptake. Am J Physiol 247:H322–H329.
Haystead TA, Sim AT, Carling D, Honnor RC, Tsukitani Y, Cohen P, Hardie DG (1989) Effects of the tumour promoter okadaic acid on intracellular protein phosphorylation and metabolism. Nature 337:78–81.
He DZ, Dallos P (1999) Somatic stiffness of cochlear outer hair cells is voltage-dependent. Proc Natl Acad Sci USA 96:8223–8228.
Holley MC, Kalinec F, Kachar B (1992) Structure of the cortical cytoskeleton in mammalian outer hair cells. J Cell Sci 102:569–580.
Horn R, Marty A (1988) Muscarinic activation of ionic currents measured by a new whole-cell recording method. J Gen Physiol 92:145–159.
Housley GD, Ashmore JF (1991) Direct measurement of the action of acetylcholine on isolated outer hair cells of the guinea pig cochlea. Proc R Soc Lond B Biol Sci 244:161–167.
Huang G, Santos-Sacchi J (1993) Mapping the distribution of the outer hair cell motility voltage sensor by electrical amputation. Biophys J 65:2228–2236.
Iwasa KH (1993) Effect of stress on the membrane capacitance of the auditory outer hair cell. Biophys J 65:492–498.
Jagger DJ, Ashmore JF (1999) Regulation of ionic currents by protein kinase A and intracellular calcium in outer hair cells isolated from the guinea-pig cochlea. Pflügers Arch 437:409–416.
Kachar B, Brownell WE, Altschuler R, Fex J (1986) Electrokinetic shape changes of cochlear outer hair cells. Nature 322:365–368.
Kakehata S, Santos-Sacchi J (1995) Membrane tension directly shifts voltage dependence of outer hair cell motility and associated gating charge. Biophys J 68:2190–2197.
Kakehata S, Santos-Sacchi J (1996) Effects of salicylate and lanthanides on outer hair cell motility and associated gating charge. J Neurosci 16:4881–4889.
Kalinec F, Holley MC, Iwasa K, Lim DJ, Kachar B (1992) A membrane-based force generation mechanism in auditory sensory cells. Proc Natl Acad Sci USA 89:8671–8675.
Koyama M, Spicer SS, Schulte BA (1999) Immunohistochemical localization of Ca^{2+}/calmodulin-dependent protein kinase IV in outer hair cells. J Histochem Cytochem 47:7–12.
Liu C, Hermann T (1978) Characterization of ionomycin as a calcium ionophore. J Biol Chem 253:5892–5894.
Mammano F, Ashmore JF (1996) Differential expression of outer hair cell potassium currents in the isolated cochlea of the guinea pig. J Physiol (Lond) 496:639–646.
Mammano F, Frolenkov GI, Lagostena L, Belyantseva IA, Kurc M, Dodane V, Colavita A, Kachar B (1999) ATP-Induced Ca^{2+} release in cochlear outer hair cells: localization of an inositol triphosphate-gated Ca^{2+} store to the base of the sensory hair bundle. J Neurosci 19:6918–6929.
Raphael Y, Wroblewski R (1986) Linkage of the submembrane cisterns with the cytoskeleton and the plasma membrane in cochlear outer hair cells. J Submicrosc Cytol 18:730–733.
Santos-Sacchi J (1991) Reversible inhibition of voltage-dependent outer hair cell motility and capacitance. J Neurosci 11:3096–3110.
Santos-Sacchi J, Dilger JP (1988) Whole cell currents and mechanical responses of isolated outer hair cells. Hear Res 35:143–150.
Santos-Sacchi J, Huang G (1998) Temperature dependence of outer hair cell nonlinear capacitance. Hear Res 116:99–106.
Santos-Sacchi J, Huang GJ, Wu M (1997) Mapping the distribution of outer hair cell voltage-dependent conductances by electrical amputation. Biophys J 73:1424–1429.
Schulte BA (1993) Immunohistochemical localization of intracellular Ca^{2+}-ATPase in outer hair cells, neurons and fibrocytes in the adult and developing inner ear. Hear Res 65:262–273.
Shehata WE, Brownell WE, Dieler R (1991) Effects of salicylate on shape, electromotility and membrane characteristics of isolated outer hair cells from guinea pig cochlea. Acta Otolaryngol 111:707–718.
Smith JB, Zheng T, Lyu R-M (1989) Ionomycin releases calcium from the sarcoplasmic reticulum and activates Na^+/Ca^{2+} exchange in vascular smooth muscle cells. Cell Calcium 10:125–134.
Szonyi M, Csermely P, Sziklai I (1999) Acetylcholine-induced phosphorylation in isolated outer hair cells. Acta Otolaryngol 119:185–188.
Tolomeo JA, Steele CR, Holley MC (1996) Mechanical properties of the lateral cortex of mammalian auditory outer hair cells. Biophys J 71:421–429.
Tunstall MJ, Gale JE, Ashmore JF (1995) Action of salicylate on membrane capacitance of outer hair cells from the guinea-pig cochlea. J Physiol (Lond) 458:739–752.
Van den Abbeele T, Tran Ba Huy P, Teulon J (1996) Modulation by purines of calcium-activated non-selective cation channels in the outer hair cells of the guinea-pig cochlea. J Physiol (Lond) 494:77–89.
Warr WB (1992) Organization of olivocochlear efferent systems in mammals. In: Auditory central nervous system (Fay RR, Popper AN, Webster DB, eds), pp 410–448. New York: Springer.
Yamamoto T, Kakehata S, Yamada T, Saito T, Saito H, Akaike N (1997) Effects of potassium channel blockers on the acetylcholine-induced currents in dissociated outer hair cells of guinea pig cochlea. Neurosci Lett 236:79–82.